

Co-targeting of VEGFR2 and PD-L1 promotes survival and vasculature normalization in pleural mesothelioma

Sophie Rovers^a, Jonas Van Audenaerde^a, Ruben Verloy^{a,b}, Jorrit De Waele^a, Louize Brants^a, Christophe Hermans^a, Ho Wa Lau^a, Céline Merlin^a, Maria Möller Ribas^{a,c}, Peter Ponsaerts^d, Steven Van Laere^a, Filip Lardon^a, An Wouters^a, Scott A. Fisher^e, Jan van Meerbeeck^{a,f,g}, Elly Marcq^{a,h,i,*}, and Evelien Smits^{a*}

^aCenter for Oncological Research (CORE), Integrated Personalized and Precision Oncology Network (IPPON), University of Antwerp, Antwerp, Belgium; ^bResearch group PLASMANT, Department of Chemistry, University of Antwerp, Antwerp, Belgium; ^cFaculty of Biology, University of Barcelona, Barcelona, Spain; ^dLaboratory of Experimental Hematology, Vaccine and Infectious Disease Institute (Vaxinfecio), University of Antwerp, Antwerp, Belgium; ^eInstitute for Respiratory Health, National Centre for Asbestos Related Diseases (NCARD), University of Western Australia, Perth, Australia; ^fMultidisciplinary Oncological Center Antwerp (MOCA), Antwerp University Hospital (UZA), Antwerp, Belgium; ^gEuropean Reference Network for Rare or Low Prevalence Lung Diseases: ERN-LUNG, ERN-LUNG Coordinating Center, Frankfurt am Main, Germany; ^hBrussels Center for Immunology, Vrije Universiteit Brussel, Brussels, Belgium; ⁱLaboratory of Dendritic Cell Biology and Cancer Immunotherapy, VIB Center for Inflammation Research, Brussels, Belgium

ABSTRACT

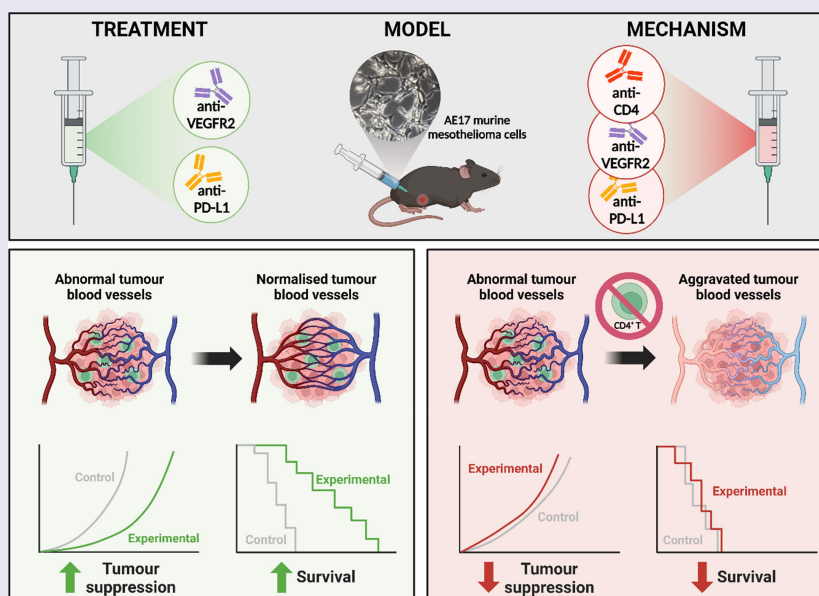
Pleural mesothelioma (PM) is an aggressive cancer caused by asbestos exposure, with limited treatment options and poor prognosis, highlighting the need for more effective therapies. Combining immune checkpoint blockade with anti-angiogenic therapy has shown potential in other cancers. Our study investigated the combined inhibition of PD-L1 and VEGFR2 in a mouse model of PM. Using C57BL/6 mice with subcutaneous AE17 mesothelioma tumors, we assessed the effects of anti-PD-L1 therapy with induction, concomitant, or consolidation anti-VEGFR2 treatment. Mice received intraperitoneal doses every three days for three treatments. Tumor growth, survival, tumor-infiltrating immune cells and intra-tumoral vasculature were analyzed. Results demonstrated that combining anti-PD-L1 with induction or concomitant anti-VEGFR2 significantly delayed tumor growth, improved survival, and promoted vascular maturation. Flow cytometry suggested T cell exhaustion in monotherapy groups, while no significant changes were seen with concomitant treatment. Depleting CD4⁺ T cells reversed the positive effects of concomitant treatment. These findings suggest that dual inhibition of PD-L1 and VEGFR2 is a promising therapeutic approach for PM, with CD4⁺ T cells playing a critical role in the immune response. This dual targeting of immune checkpoints and angiogenesis offers a potential new avenue for improving outcomes in PM treatment and warrants further clinical exploration.



ARTICLE HISTORY

Received 20 January 2025
Revised 14 May 2025
Accepted 21 May 2025


KEYWORDS

Anti-angiogenesis; cancer immunotherapy; combination therapy; immune checkpoint blockade; pleural mesothelioma



CONTACT Sophie Rovers  Sophie.Rovers@uantwerpen.be  Center for Oncological Research (CORE), Integrated Personalized and Precision Oncology Network (IPPON), University of Antwerp, Antwerp, Belgium

*Shared senior author.

 Supplemental data for this article can be accessed online at <https://doi.org/10.1080/2162402X.2025.2512104>.

© 2025 The Author(s). Published with license by Taylor & Francis Group, LLC.

This is an Open Access article distributed under the terms of the Creative Commons Attribution-NonCommercial License (<http://creativecommons.org/licenses/by-nc/4.0/>), which permits unrestricted non-commercial use, distribution, and reproduction in any medium, provided the original work is properly cited. The terms on which this article has been published allow the posting of the Accepted Manuscript in a repository by the author(s) or with their consent.

1. Introduction

Pleural mesothelioma (PM) is an aggressive tumor affecting the pleura that is commonly attributed to asbestos exposure.^{1,2} As of today, 144 out of 198 countries have not yet banned the use of asbestos. With all member states of the European Union implementing an asbestos ban by 2005, PM incidence reached its predicted peak around 2020, thus garnering a lot of interest in recent years.^{1,3,4} Given the median latency period of approximately 30–40 years and the forecasted 4% annual increase in asbestos exposure among construction workers until 2031, the global mesothelioma burden is predicted to worsen.^{1,3,5,6} For over 20 years, the first-line treatment for PM patients has consisted of a combination of platinum-based chemotherapy (cisplatin or carboplatin) with an antifolate (pemetrexed or raltitrexed). However this regimen has improved the median overall survival (OS) to merely 12–14 months compared to 6–9 months when left untreated.^{7,8} With the recent introduction of dual immunotherapy as standard-of-care treatment in PM, prognosis further improved to a median of 18 months which is still poor for the large majority of patients.⁹ Improved treatment strategies are therefore urgently needed.

The development of new immunotherapies targeting immune checkpoints has significantly advanced since the first FDA-approval of ipilimumab in 2011, followed by pembrolizumab and nivolumab in 2014.¹⁰ The CheckMate743 trial, which resulted in the approval of combined ipilimumab + nivolumab as first-line treatment for PM, represents a pivotal moment for immunotherapy in mesothelioma,⁹ while a multitude of other immune checkpoint blockade (ICB) strategies are still being investigated in preclinical and clinical trials.¹¹

In addition, therapies targeting other pathways involved in mesothelioma pathogenesis, such as anti-angiogenic agents, have also been studied extensively in recent clinical trials in various combination strategies.^{12–14} As a cancer hallmark, angiogenesis is an attractive target for cancer therapy. The pro-angiogenic vascular endothelial growth factor receptor 2 (VEGFR2) is known to be highly expressed in malignant epithelial mesothelioma¹⁵ and has been explored as a potential therapeutic target in preclinical models of PM, as well as in clinical trials. The small molecule inhibitor nintedanib was shown to have significant anti-tumor effects in mesothelioma *in vitro* and *in vivo*,¹⁶ but ultimately failed to improve progression-free survival (PFS) of PM patients when combined with standard-of-care chemotherapy in the phase 3 LUME-Meso trial.¹³ In the phase 2 RAMES trial, a monoclonal antibody (mAb) targeting VEGFR2 (ramucirumab) was found to significantly improve OS when used in combination with gemcitabine as a second-line treatment for PM.¹⁴ Interestingly, anti-angiogenic strategies and ICB have also been shown to enhance each other's efficacy in various solid tumor models.^{17,18} In mesothelioma, the mAb bevacizumab, which targets VEGF, has recently been studied in combination with the anti-PD-L1 agent atezolizumab and chemotherapy in the BEAT-meso trial (NCT03762018). However, this trial failed to meet its primary endpoint of significantly improving OS with this treatment arm (20.5 months versus 18.1 months with bevacizumab + chemotherapy, $p = 0.14$; data presented at the

ASCO Annual Meeting 2024), underscoring the need for further preclinical research. In particular, preclinical investigation of monoclonal antibodies targeting VEGFR2 could shed more light on the best combination regimen and its mechanism of action in mesothelioma.

As we have previously demonstrated a survival benefit for blockade of PD-L1 in a mouse model of PM,¹⁹ the primary objective of this study was to determine the therapeutic effects of combined blockade of PD-L1 and VEGFR2. A secondary objective was to assess the effects of this combination treatment on the intratumoural vasculature and the tumor immune microenvironment (TIME), to elucidate the underlying mechanisms of the potentially enhanced therapeutic effect.

2. Methods

2.1. Cell lines

Murine AE17 epithelioid mesothelioma cells were maintained in RPMI 1640 medium (Gibco®, Life Technologies, Belgium) supplemented with 10% fetal bovine serum (FBS) and 2 mM L-glutamine (Gibco®, Life Technologies, Belgium). This PM cell line was kindly provided by our collaborator Dr. Scott Fisher from the Tumor Immunology Group at the National Centre for Asbestos Related Diseases (NCARD) at the University of Western Australia in Perth. Cells were harvested with TrypLE (Gibco®, Life Technologies, Belgium), washed twice in sterile phosphate buffered saline (PBS), and counted prior to *in vivo* inoculation. Cell viability was assessed by trypan blue exclusion assay and only suspensions with a viability of >95% were used.

2.2. Mice

Female C57BL/6J mice (6–8 weeks) were bought from Charles River Laboratories (Saint-Germain-Nuelles, France) and maintained under standard housing conditions at the animal facility of the University of Antwerp. All experiments were conducted in accordance with the University of Antwerp animal ethics guidelines (Ethical Committee for Animal Testing, University of Antwerp, Belgium, approval number ECD 2019–32) and with the European code for the care and use of laboratory animals and the ARRIVE guidelines. Sample size calculations were performed using the statistical software package G*power. The effect size was calculated based on preliminary experiments. A significance level of $p < 0.05$ was used to calculate the sample size of n mice per group. In total, 319 mice were used during this study. Animals were excluded from analysis if humane endpoints were met before the end of treatment and outliers were identified and excluded using the ROUT method.

2.3. Tumour cell inoculation

Mice were inoculated subcutaneously (s.c.) into the shaved left flank with 0.5×10^6 AE17 cells in 100 μ L PBS using a 27 G needle. A calliper was used to monitor tumor size. Tumor

volume in cubic millimeters (mm^3) was determined using the following formula: $\frac{\text{Length} \times \text{Width}^2}{2}$.

Mice were euthanized once tumor volume exceeded 936 mm^3 , in accordance with animal ethics guidelines.

2.4. Immune checkpoint and angiogenesis blocking antibodies *in vivo*

All our *in vivo* antibodies were bought from BioXCell: anti-VEGFR2 (clone DC101) and anti-PD-L1 (clone 10F.9G2). The concentration of the anti-PD-L1 antibody (200 μg ; 10 mg/kg) and the treatment schedule (1 dose every 3 days for a total of 3 doses; q3dx3) was based on the literature²⁰ and was previously validated *in vivo*.¹⁹ The concentration of the anti-VEGFR2 antibody was determined *in vivo* after titration (100 μg , 200 μg , 400 μg , 800 μg), with the maximum dose (800 μg ; 40 mg/kg) being based on literature.²¹ Blocking antibodies were administered via intraperitoneal (i.p.) injection at the appropriate dose diluted in 100 μL PBS per mouse.

2.5. Frozen tissue sectioning

Tumors were harvested at endpoint ($\geq 936 \text{ mm}^3$) and maintained in a 10% sucrose solution for 1 hour at 4°C before being transferred to a 30% sucrose solution and left at 4°C overnight. Tumors were then placed in embedding molds, covered in Tissue-VECTASHIELD® O.C.T.™ embedding medium (Sakura Finetek Europe B.V., Netherlands), and immersed in ice-cold isopentane for 3 minutes before being frozen down to -80°C .²² Frozen tissue sections of 5 μm were made using a cryostat and were fixed for 10 minutes in ice-cold acetone. For each treatment group, 3 tumors were randomly selected for further analysis and tissue sections were made at the 25%, 50%, and 75% regions of the tumors to get data representative of the whole tumor. Tissue sections were preserved at -80°C .

2.6. Immunofluorescence

Pre-fixed frozen tissue sections were fixed again for 10 minutes in ice-cold acetone. After being left to air-dry, an IHC PAP pen (Enzo Life Sciences BVBA, Belgium) was used to create a hydrophobic barrier around the tissue sections. Following a washing step using PBS, blocking buffer (PBS with 10% FBS and 1% BSA) was added to the sections for 1 hour at room temperature. The tissues were then incubated with a primary antibody solution in a humid chamber and left overnight at 4°C .²² The primary antibodies used in this study include: Rat anti-mouse CD31 (clone MEC 13.3, dilution 1:100, BD Biosciences, Belgium); Rabbit polyclonal anti-CA9 (dilution 1:1500, Novus Biologicals, UK); and Rabbit polyclonal anti- αSMA (dilution 1:100, Novus Biologicals). Tissues were then washed three times in PBS and incubated with fluorescent labeled secondary antibodies for 1 hour at room temperature in a dark humid chamber. The following fluorescent conjugated secondary antibodies were used: Donkey anti-rat AF594 (red, dilution 1:3000, ThermoFisher Scientific, Belgium); and Goat anti-rabbit AF488 (green, dilution 1:200 for CA9 detection and 1:500 for αSMA detection, Abcam, UK). Negative controls consisted of tissues stained with a secondary antibody,

but not a primary antibody. The tissues were then washed 3 times for 5 minutes in a PBS-filled beaker. Finally, we added 30 μL of VECTASHIELD® HardSet Antifade Mounting Medium with DAPI (Vector Laboratories, Belgium) per tissue section, and covered the tissues with a coverslip. The mounting medium was allowed to harden for 15 minutes at room temperature, after which the slides were kept at 4°C in the dark until image acquisition on a reflected light fluorescence microscopy system (Olympus BX51) with the CellSens Dimension software. For each tumor section, 4 representative images were taken at 10 \times magnification. Further analysis of the images was carried out using ImageJ, the IKOSA® Network Formation Assay (v2.2.0), and GraphPad Prism (v10.2.1).

2.7. Preparation of single cell suspensions

For the flow cytometric characterization of the immune cell populations in the TIME, single-cell suspensions were made from tumors harvested 24 hours after the final treatment. After harvesting, tumor tissue was minced as small as possible using a scalpel and suspended into tumor digestion medium (FACS buffer [Sheath fluid + 10 mg/mL BSA + 20 mg/mL NaN_3] + 0.2 mg/mL DNA-se + 1.5 mg/mL collagenase type IV). Tumors were then incubated for 30 minutes at 37°C and 5% CO_2 on a tube rocker. After incubation, the tumor tissue was passed through a 40 μm cell strainer (VECTASHIELD®, Netherlands). Tumor cell suspensions were washed with FACS buffer to remove any remaining traces of digestion medium, after which they were ready for further downstream applications.

2.8. Flow cytometry

The effect of the different (combination) treatment strategies on the immune cell composition of the *in vivo* TIME was investigated using a multicolor flow cytometry panel. Single cell suspensions from *in vivo* tumors were stained using the following anti-mouse mAbs: CD45.2-AlexaFluor700 (clone 104), CD3-BV510 (clone 17A2), CD4-PerCP-Cy5.5 (clone GK1.5), CD8a-BV570 (clone 53-6.7), CD335-BV605 (clone 29A1.4), I-A/I-E-BV650 (clone M5/114.15.2), CD25-BV785 (clone PC61), CD11c-FITC (clone N418), CD278-PE-Dazzle594 (clone C398.4A), CD274-PE-Cy7 (clone MIH7), CD279-BV421 (clone 29F.1A12), CD309-PE (clone 89B3A5), and FOXP3-APC (clone MF-14; intracellular), which were all purchased from VECTASHIELD® (Netherlands). The LIVE/IKOSA® Fixable Near-IR Stain from Tek® (ThermoFisher Biolegend®) was used to stain dead cells. FMO controls were also included. The NovoCyte Quanteon flow cytometer with NovoExpress software was used for sample acquisition, and further analysis was carried out using FlowJo (v10.10.0) and GraphPad Prism.

2.9. Immune cell depletion

To investigate the role of different immune cell populations, we functionally depleted specific immune cell types. Mice were subcutaneously injected with AE17 cells as described above. CD8^+ , CD4^+ , and regulatory T cells were depleted using 200 μg of anti-CD8 (Clone YTS 196.4, BioXCell), anti-CD4 (Clone GK1.5, BioXCell), or anti-

CD25 (Clone 7D4 (non-IL-2 blocking), Absolute Antibody, UK) mAbs, respectively. Two different isotype controls were included: Rat IgG2b anti-keyhole limpet hemocyanin (Clone LTF-2, BioXCell) for anti-CD8 and anti-CD4, and Mouse IgG2a anti-fluorescein (Clone 4-4-20 (enhanced), Absolute Antibody) for anti-CD25. Mice were randomized into 7 different treatment groups¹: PBS control²; anti-PD-L1 + anti-VEGFR2³; anti-PD-L1 + anti-VEGFR2 + anti-CD8⁴; anti-PD-L1 + anti-VEGFR2 + anti-CD4⁵; anti-PD-L1 + anti-VEGFR2 + anti-CD25⁶; anti-PD-L1 + anti-VEGFR2 + IgG2a isotype control; and⁷ anti-PD-L1 + anti-VEGFR2 + IgG2b isotype control. Depletion antibodies or isotype control were administered i.p. on days -1, 0, 3, and 6 of the treatment schedule. Tumour growth and survival were followed up as described above. On day 1, a depletion check was performed via flow cytometric analysis on 5 μ L of blood collected from the tail vein.

2.10. TCGA data analysis

Gene and protein expression (respectively counts and z-scores) data and clinicopathological characteristics (i.e. survival data) for a series of 87 patients with PM (TCGA Firehose Legacy) were retrieved from the cBioPortal for Cancer Genomics (<https://www.cbioportal.org>). Gene expression data were normalized using the variance stabilizing transformation (VST) algorithm of the BioC-package *DESeq2*. VST-normalized gene expression data were used to calculate abundance scores for various cell types using the BioC-package *ConsensusTME* with marker gene sets specific for PM. The tumor inflammation score (TIS²³) was calculated using gene set variation analysis (BioC-package *GSVA*) with a Gaussian kernel to estimate the cumulative distribution function. Spearman correlations between VEGFA, KDR (VEGFR2), CD274 (PD-L1), PDCD1 (PD-1) gene expression, VEGFR2 protein expression, TIS values and regulatory T cell abundance scores were calculated and visualized using the R-package *rstatix*. Univariate Cox regression analyses for disease-specific, disease-free, progression-free, and overall survival were performed using the R-package *survival*. Kaplan-Meier plots were visualized using the R-package *survminer*. Correlation analysis and visualization was performed using the R-package *rstatix*, and univariate and multivariate interaction models were constructed with base R-functions. Likelihood-ratio tests were performed with the R-package *lmerTest*.

2.11. Statistics

Kaplan-Meier curves were created for *in vivo* survival data and a log-rank (Mantel-cox) test was performed to detect any statistical differences between the different treatment groups.

To analyze differences in tumor kinetics over time, we used R with the *afex* and *emmeans*²⁴ packages to perform mixed model ANOVAs.

Significant differences in marker expression between treatment groups as assessed by flow cytometry or

immunofluorescence were investigated with a Tukey's multiple comparisons test. *P*-values ≤ 0.05 were considered statistically significant. *p*-values < 0.1 were considered as trending toward statistical significance. GraphPad Prism was used for statistical analyses.

3. Results

3.1. Inhibition of VEGF-VEGFR2 signalling significantly slows tumour growth and improves survival in a mesothelioma mouse model

Through the analysis of data from 87 pleural mesothelioma patients available on the Cancer Genome Atlas (TCGA), we were able to identify an association between VEGFR2 protein expression and poor survival outcomes. Using Cox regression analysis, we found that patients with high VEGFR2 protein expression had significantly worse PFS (hazard ratio (HR) = 1.647, *p* = 0.013), and disease-specific survival (DSS; HR = 1.44, *p* = 0.004) outcomes compared to those with low VEGFR2 protein expression, whereas no associations with OS (*p* = 0.117) or disease-free survival (*p* = 0.090) were found (Supplementary figure S1). When dichotomizing VEGFR2 protein expression levels relative to the median, the above associations were confirmed through Kaplan-Meier analysis (Figure 1 a,b). Notably, no associations between VEGFR2, or VEGFA mRNA expression levels and any of the evaluated survival endpoints were observed (Supplementary figure S1), despite significant correlation between these parameters and VEGFR2 protein expression (Figure 1c). Together, these data solidify VEGFR2 as an interesting potential target for anti-cancer therapy in PM.

To explore how combined targeting of VEGFR2 and PD-1/PD-L1 might affect the TIME, we evaluated correlations amongst VEGFR2 mRNA (KDR) and protein expression, mRNA expression of VEGFA, CD274 (PD-L1), and PDCD1 (PD-1), and tumor inflammation scores (TIS) (Figure 1c). TIS values are significantly correlated with CD274 and PDCD1 mRNA expression but not with VEGFA mRNA or VEGFR2 mRNA/protein expression. We then explored if tumor inflammation can be better explained by considering interactions between expression values of VEGFA/VEGFR2 on the one hand, and CD274/PDCD1 on the other hand. Our results (Supplementary figure S2) demonstrate that the interaction terms of PDCD1 mRNA expression, but not CD274 mRNA expression, with any of the VEGF-related expression values are associated with higher TIS values (i.e. interaction PDCD1 mRNA and VEGFR2 protein: OR = 1.243, *p* = 0.003; interaction PDCD1 and VEGFR2 mRNA: OR = 1.555, *p* = 0.013; interaction PDCD1 and VEGFA mRNA: OR = 1.086, *p* = 0.074). Likelihood-ratio tests reveal that the multivariate interaction models containing VEGFR2 expression values better explain TIS values as compared to the univariate models containing only PDCD1 mRNA expression (VEGFR2 protein: *p* = 0.006; VEGFR2 mRNA: *p* = 0.017; VEGFA: *p* = 0.169). Subgroup analysis comparing TIS values to PDCD1 expression in PM samples with high and low VEGFR2 protein expression, dichotomized relative to zero, indeed reveal a stronger correlation in the VEGFR2-high group (Figure 1d). Interestingly, high TIS scores have been linked to better clinical sensitivity to

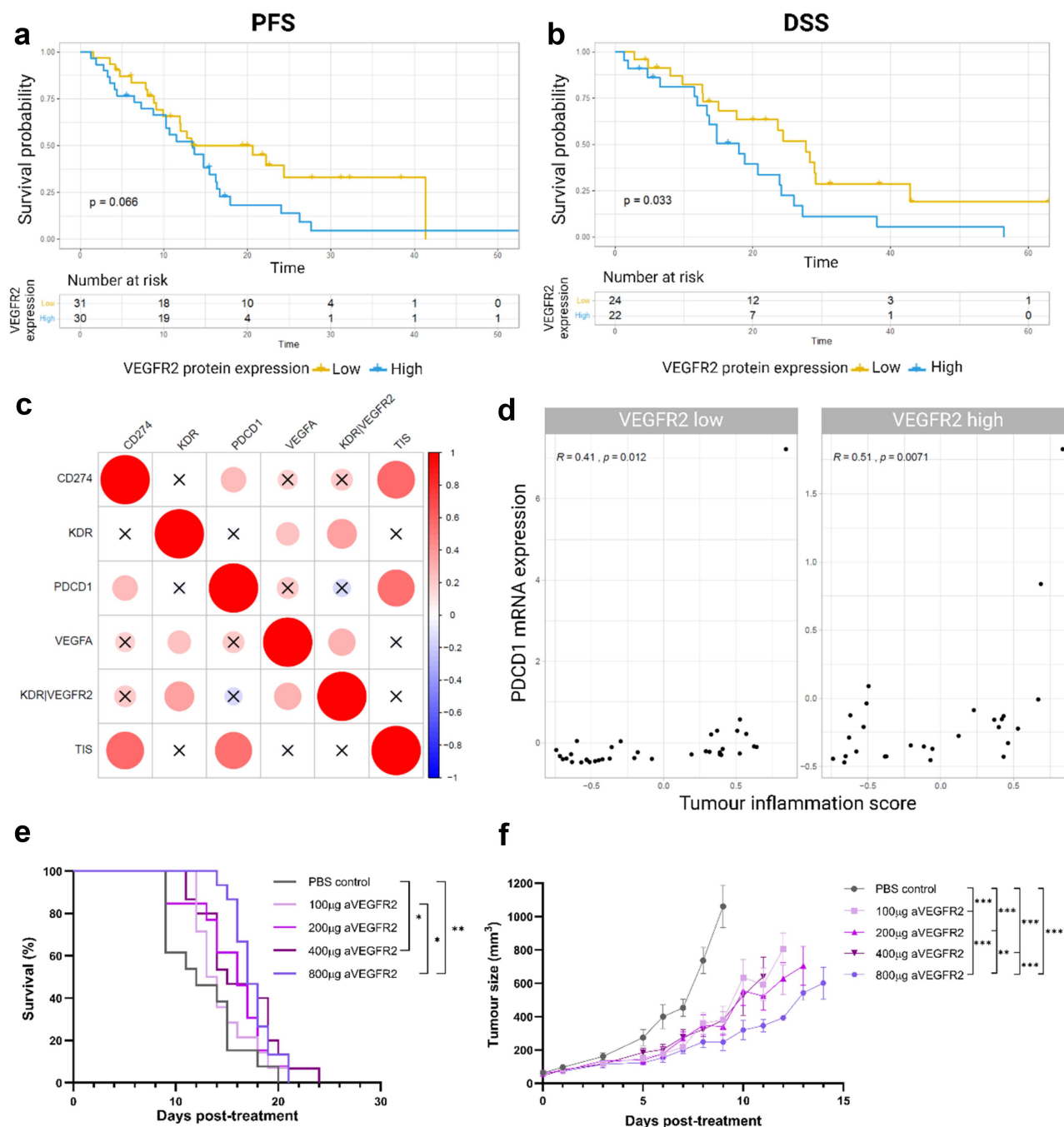


Figure 1. Anti-VEGFR2 monoclonal antibody delays tumour growth and extends survival of the AE17 C57BL/6 PM mouse model. (a–b) Kaplan-Meier curves showing (a) the progression-free survival (PFS) and (b) the disease-specific survival (DSS) of 87 pleural mesothelioma patients in function of their VEGFR2 protein expression level. (c) bubble plot showing the correlations between CD274 (PD-L1), KDR (VEGFR2), PDCD1 (PD-1), and VEGFA gene expression, VEGFR2 protein expression, and tumour inflammation signature (TIS) scores. (d) correlation analysis between PDCD1 mRNA expression and TIS within VEGFR2-low (left) and VEGFR2-high (right) subgroups. (e) Kaplan-Meier curve showing the survival of mice treated with increasing doses of anti-VEGFR2 mAb or PBS control. Pooled data from three independent experiments ($n = 15$ mice per group). Statistical significance was determined using a log-rank test. (f) tumour growth curves from mice treated with increasing doses of anti-VEGFR2 mAb or PBS control. Tumour size (mm³) as measured over time from the start of treatment (day 0) until the first mouse of each group was euthanised. Mice were treated every third day for a total of three doses (q3dx3). Statistical significance was determined using a mixed model ANOVA. Error bars represent the mean \pm SEM. Data representative of three independent experiments ($n = 5$ mice per group). * $p < 0.05$, ** $p < 0.01$, *** $p < 0.001$.

ICB.²⁵ Together, these results highlight the complex entanglement of the VEGF/VEGFR2 and PD-1/PD-L1 pathways in shaping the TIME of PM.

In the present study, we first performed a dose titration of an anti-VEGFR2 mAb in the AE17 C57BL/6 model of pleural mesothelioma. Compared to the untreated control, we observed a statistically significant survival benefit with the

administration of 400 µg and 800 µg of anti-VEGFR2 mAb, but not with 100 µg or 200 µg (Figure 1e). In addition, there was a significant delay in tumor growth with all different doses compared to the control group (Figure 1f). In concordance with the prolonged survival even compared to the 100 µg dose, the 800 µg dose also achieved the most substantial deceleration of tumor growth, differing significantly from all the other

lower doses (Figure 1f). These findings, in conjunction with existing literature,²¹ provided the rationale for selecting the 800 µg dosage of the anti-VEGFR2 mAb for subsequent pre-clinical investigation and potential combination with ICB.

3.2. Combination of anti-PD-L1 with anti-VEGFR2 as induction or concomitant treatment slows tumour growth and improves survival

We next sought to explore the effect of combining an anti-VEGFR2 mAb with another antibody targeting the immune checkpoint molecule PD-L1. In a previous study, we observed a delay in tumor growth and significant survival benefit with PD-L1-targeting therapy in the AB1 hA BALB/c PM mouse model.¹⁹ In the current study utilizing the AE17 C57BL/6 model, we adopted a similar approach with an anti-PD-L1 mAb dosage of 200 µg/mouse administered every third day for a total of 3 doses (q3dx3).

As in Figure 1, C57BL/6 mice were subcutaneously inoculated with AE17 murine mesothelioma cells subjected to treatment with PBS control, anti-VEGFR2 or anti-PD-L1 monotherapy, or a combination regimen where anti-VEGFR2 was administered as induction (prior to ICB), concomitant (with ICB), or consolidation (after ICB) therapy (Figure 2a). We noted a significant delay ($p < 0.05$) in tumor growth with all treatment regimens compared to the PBS control group (Figure 2c and d). Interestingly, the concomitant treatment cohort (light blue lines) exhibited a longer delay in tumor growth compared to both the anti-PD-L1 monotherapy ($p < 0.001$) and the consolidation treatment ($p = 0.009$) groups. Furthermore, survival analysis indicated a notable survival benefit only for the anti-VEGFR2 monotherapy and its combination with anti-PD-L1 when administered as induction or concomitant therapy (Figure 2b). Our findings revealed a significant improvement in survival among mice treated with the combination therapy (either as induction or concomitant therapy) compared to those receiving anti-PD-L1 monotherapy ($p = 0.0001$ and $p = 0.0018$, respectively) or the consolidation regimen ($p = 0.0012$ and $p = 0.0064$, respectively). Notably, despite the lack of statistical significance, there was a discernible trend toward enhanced survival in both the concomitant ($p = 0.09$) and induction ($p = 0.08$) groups compared to anti-VEGFR2 monotherapy. We conclude that the combination of anti-VEGFR2 with anti-PD-L1 leads to a significant delay in tumor growth and longer survival when anti-VEGFR2 is administered as induction or concomitant therapy, but not as consolidation therapy.

3.3. Normalisation of tumour vasculature by combined anti-PD-L1 and anti-VEGFR2 treatment

We hypothesized that the observed enhanced effects of combined treatment may be a consequence of blood vessel normalization and subsequent immune microenvironment reprogramming. Therefore, we collected and cryopreserved tumors from mice treated with the treatment schedules depicted in Figure 2a and performed immunofluorescent imaging of endothelial cell marker CD31, pericyte marker α SMA (Figure 3a, Supplementary figure S3A), and hypoxia marker CA9 (Supplementary figure S3B and C). The VECTASHIELD®

tube formation analysis software was used to quantitatively evaluate various important characteristics of a mature vascular network (endothelial cell-covered area, number of branching points, number of loops, and total vessel length). ImageJ software was used to evaluate CD31- α SMA co-localization as a marker of pericyte coverage, indicative of vessel normalization.²⁶

We observed significantly increased CD31 expression in tumors subjected to anti-PD-L1 monotherapy or combined with concomitant or induction VEGFR2 blockade when compared to the other treatment groups (Figure 3b-c). In addition, while tumors in the anti-VEGFR2 monotherapy and consolidation groups displayed a notable diminution of branching points and blood vessel length, the concomitant treatment significantly improved these attributes (Figure 3b-c). Both the induction and concomitant regimens also significantly increased the presence of blood vessel loops, suggestive of a more mature vascular network (Figure 3b-c). Interestingly, analysis of alpha-SMA expression revealed a significantly higher percentage of CD31-positive cells co-localizing with alpha-SMA-positive cells in the induction therapy group, indicating an increase in pericyte coverage of the blood vessels (Figure 3b-c). No significant changes in CA9 expression were identified (Supplementary figure S3B and C). Overall, our findings led us to conclude that the anti-VEGFR2 monotherapy and consolidation groups did not exhibit any indications of vessel normalization. Conversely, the induction and concomitant modalities revealed several traits suggestive of a more mature and functional vascular network, with the concomitant treatment demonstrating 4 out of the 6 distinctive characteristics evaluated.

3.4. Concomitant anti-VEGFR2 and anti-PD-L1 therapy sustains immune stability in a mesothelioma model

Next, as combined therapy appeared to normalize the intratumoural vasculature, we hypothesized that this might lead to increased tumor infiltration of immune cells. Therefore, to assess whether combination treatment also affected the TIME, we performed flow cytometric analyses on tumors to determine the presence and expression profiles of different immune cell populations (Figure 4a, Supplementary figure S4). Tumors treated with anti-PD-L1 or anti-VEGFR2 monotherapy were significantly smaller compared to control and the induction anti-VEGFR2 setting at the time of euthanasia (Figure 4b). While there were no significant differences in the number of CD45⁺ immune cells across any of the treatment groups (Figure 4c), we did observe notable variances in the presence of some specific immune cell subsets. The number of dendritic cells (DCs) per mg of tumor tissue was significantly elevated in the anti-PD-L1 and anti-VEGFR2 monotherapy groups compared to control and the combination treatments (Figure 4d), whereas no differences were found in the natural killer (NK) cell population (Figure 4e). Total T cell presence was significantly higher in the anti-VEGFR2 monotherapy group (Figure 4f), and further analysis revealed that both CD8⁺ T cells, CD4⁺ T helper cells, and regulatory T cells (Tregs) were specifically increased in this group (Figure 4h-j). We also identified a CD3-positive, CD4- and CD8-negative

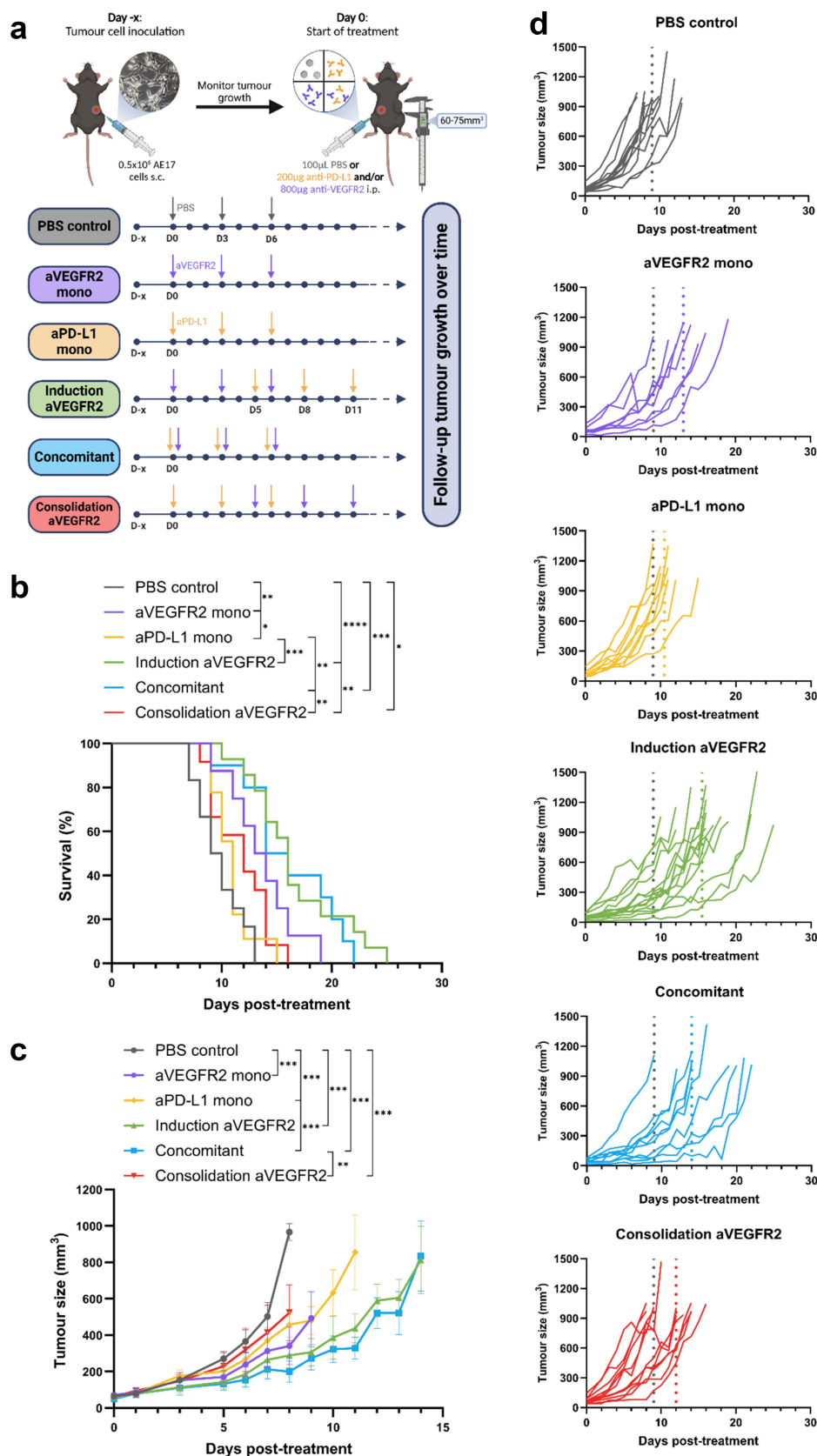


Figure 2. Combined treatment with anti-VEGFR2 and anti-PD-L1 slows tumour growth and conveys a survival benefit in the AE17 C57BL/6 mesothelioma mouse model. (a) schematic of the *in vivo* experimental set-up and treatment timelines. (b) Kaplan-Meier curves showing the post-treatment survival of mice treated with the indicated therapies. Pooled data from three independent experiments ($n = 8-14$ mice per group). Statistical significance was determined using a log-rank test. (c) tumour growth curves from mice treated as indicated. Tumour size (mm³) was measured over time from tumour inoculation and is shown here from the day of start of treatment until the first mouse of each group was euthanised. Statistical significance was determined using a mixed model ANOVA. Error bars represent the mean \pm SEM. Data representative of at least three independent experiments ($n = 3-5$ mice per group). (d) spaghetti plots showing tumour kinetics data, with each line representing an individual mouse within the different treatment groups. The grey dotted line at day 9 post-treatment represents the timepoint at which 50% of the control animals had reached their humane endpoint; the coloured dotted lines represent the timepoints at which 50% of animals of each individual group reached their humane endpoint. $*p < 0.05$, $**p < 0.01$, $***p < 0.001$, $****p < 0.0001$. Created with BioRender.com.

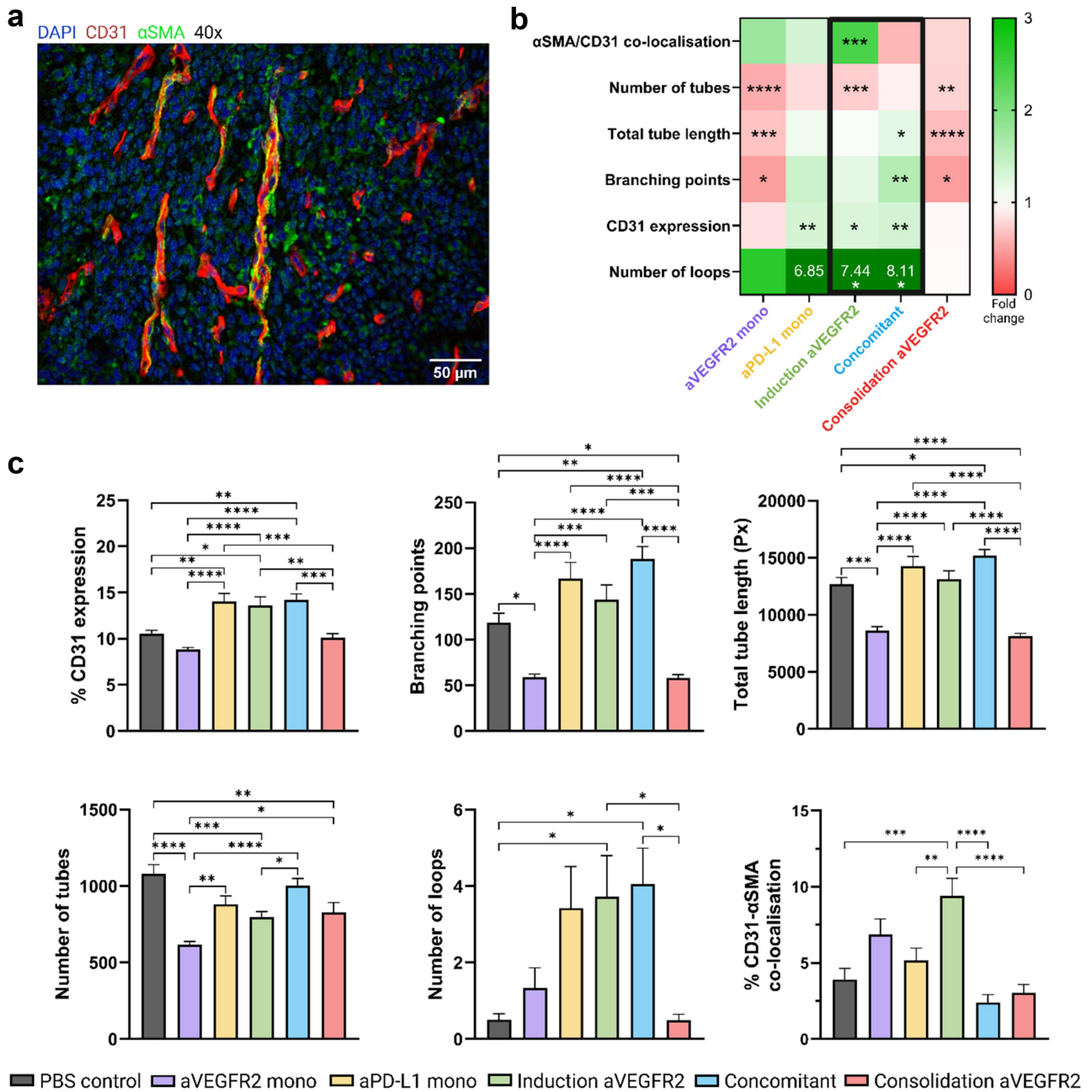


Figure 3. Intratumoural vasculature in AE17 C57BL/6 mice is normalised by combined anti-VEGFR2 and anti-PD-L1 treatment. (a) Representative immunofluorescence image of tumour tissue stained for CD31 (red), α SMA (green), and DAPI (blue), 40x magnification. (b) heatmap of VECTASHIELD® and ImageJ analysis results expressed as the Fold change normalised to the PBS control group. (c) VECTASHIELD® quantification of: percentage of CD31 expression (top left); number of branching points (top middle); total tube length expressed in pixels (px) (top right); number of tubes (bottom left); number of loops (bottom middle). Quantification of CD31- α SMA co-localisation, expressed as the percentage of CD31-positive cells covered in α SMA-positive cells (yellow signal) (bottom right). Error bars represent the mean \pm SEM. Statistical significance was determined by one-way ANOVA with Tukey's multiple comparisons test. * $p < 0.05$, ** $p < 0.01$, *** $p < 0.001$, **** $p < 0.0001$.

double-negative T (DNT) cell population (Figure 4g), as well as a CD25⁺ FoxP3⁺ subset of Tregs (Figure 4k), but neither cell type presented any significant changes in numbers. In addition, when comparing the expression levels of PD-1, PD-L1, and ICOS on the different immune cell populations, we found an increased expression of PD-1 on CD8⁺ T cells in both monotherapy groups and the consolidation anti-VEGFR2 group that could be suggestive of T cell exhaustion (Figure 4l). Furthermore, ICOS expression was significantly higher on Tregs in the monotherapy groups. As Tregs are commonly associated with immunosuppression, this observation is

consistent with our *in vivo* findings where the monotherapies demonstrated inferior efficacy compared to the combination therapy (Figure 2). PD-L1 expression was upregulated on DCs and NK cells across all treatment groups. Surprisingly, the induction treatment group displayed an expression profile similar to that of the consolidation treatment group, with significantly heightened PD-1 expression on DCs as well as elevated ICOS expression on CD8⁺ T cells and Tregs, indicative of immune response regulation (Figure 4l). In light of these findings and in consideration of the potential future clinical implementation of this treatment, we decided to continue with

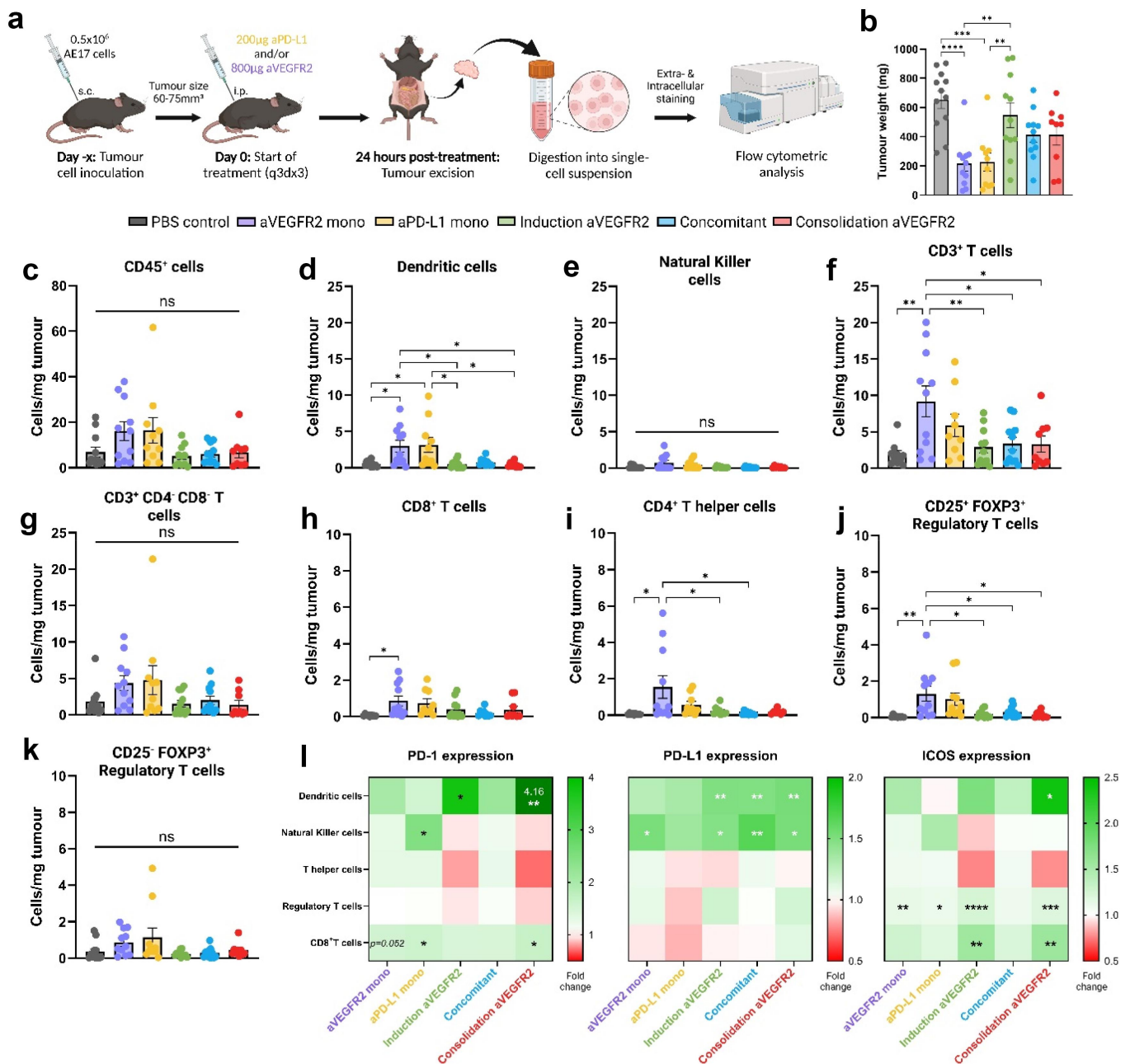


Figure 4. The complex tumour immune microenvironment of the AE17 C57BL/6 mesothelioma mouse model treated with anti-VEGFR2 and/or anti-PD-L1 therapy. (a) schematic detailing the experimental setup. Experiment repeated twice with a total of $n = 9-12$ mice per group. (b) tumour weights in milligram (mg) with mean \pm SEM. Dots represent individual tumours. (c-k) quantification of CD45.2⁺ cells (leukocytes) (c), CD45.2⁺ CD3⁺ NKp46⁺ CD11c⁺ MHCII⁺ dendritic cells (d), CD45.2⁺ CD3⁺ NKp46⁺ natural killer cells (e), CD45.2⁺ CD3⁺ T cells (f), CD45.2⁺ CD3⁺ CD4⁺ CD8⁺ double-negative T cells (g), CD45.2⁺ CD3⁺ CD8⁺ T cells (h), CD45.2⁺ CD3⁺ CD4⁺ FOXP3⁺ CD25⁺ Th cells (i), CD45.2⁺ CD3⁺ CD4⁺ FOXP3⁺ CD25⁺ Tregs (j), and CD45.2⁺ CD3⁺ CD4⁺ FOXP3⁺ CD25⁺ Tregs, expressed as the absolute number of cells per mg of tumour tissue. Error bars represent the mean \pm SEM and dots represent individual tumours. (l) heatmaps of the percentage of PD-1- (left), PD-L1- (middle) and ICOS-expressing (right) immune cells expressed as the Fold change normalised to the PBS control group. Statistical significance was determined by one-way ANOVA with Tukey's multiple comparisons test. * $p < 0.05$, ** $p < 0.01$, *** $p < 0.001$, **** $p < 0.0001$. Created with BioRender.com.

the concomitant combination approach in further experiments.

3.5. CD4⁺ T cells are critical for anti-VEGFR2 and anti-PD-L1 therapy efficacy

To further understand the role of the different T cell populations found within the TIME, we depleted these cells *in vivo* and investigated the impact on treatment outcome. As depicted in Figure 5a, mice with subcutaneous AE17 tumors received

injections of mAbs targeting CD8, CD4, or CD25 (non-IL-2 blocking), and were treated with concomitant anti-VEGFR2 and anti-PD-L1. Depletion efficacy was assessed via flow cytometry on day 1, confirming successful ablation of CD8⁺ T cells, CD4⁺ T cells, and Tregs, respectively (Supplementary figure S5).

Depletion of CD8⁺ T cells did not significantly affect tumor growth ($p = 0.971$) or survival ($p = 0.0964$) compared to the concomitant treatment group, although there was a trend toward reduced survival benefit (Figure 5b-c). On the other

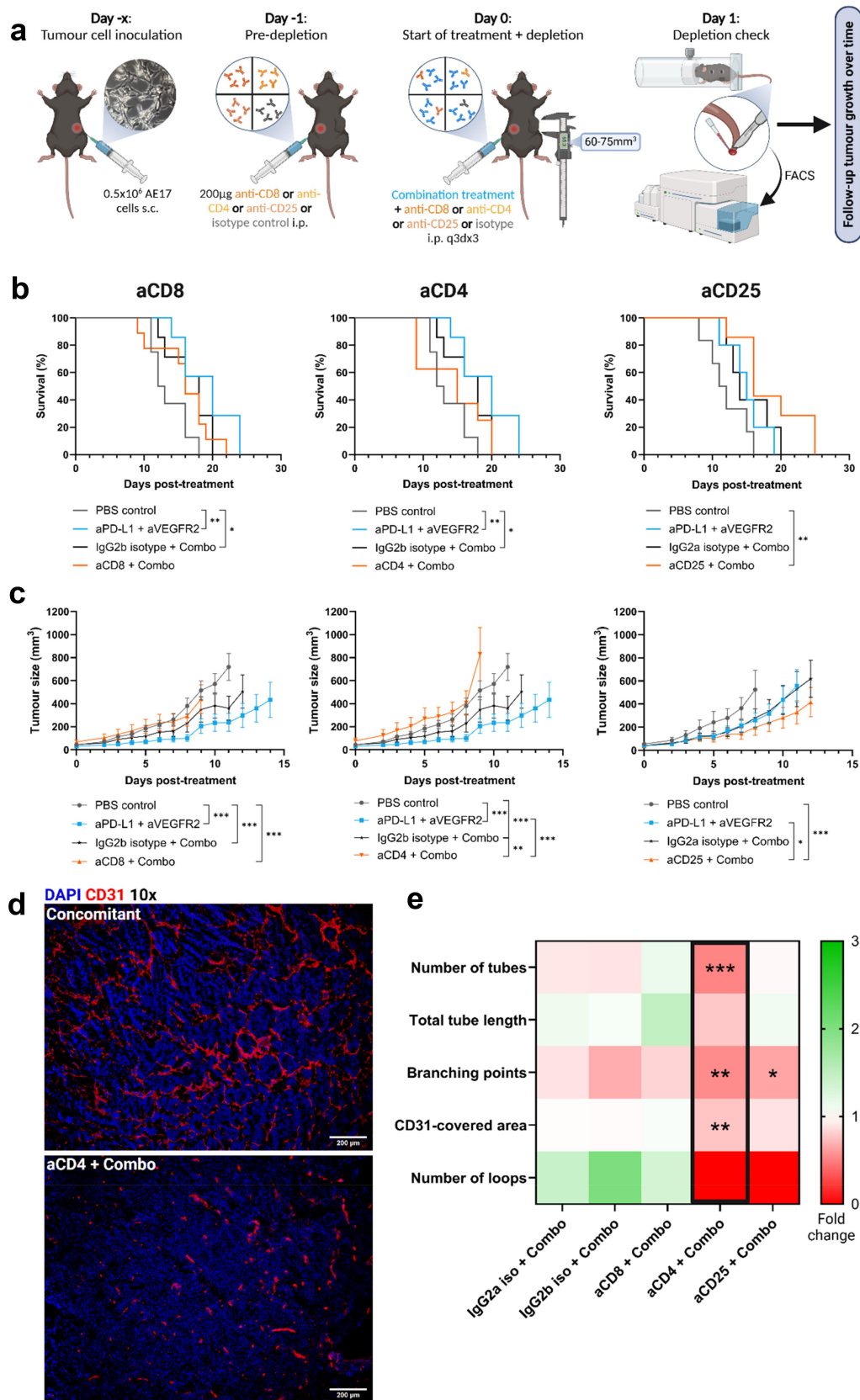


Figure 5. Depletion of CD4⁺ T cells reverses therapeutic effects of combined anti-VEGFR2 and anti-PD-L1 treatment and abrogates intratumoural vasculature. (a) schematic of the experimental design and timeline. (b) Kaplan-Meier curves showing the post-treatment survival of mice treated with concomitant anti-VEGFR2 and anti-PD-L1 treatment (combo) as well as CD8⁺ (left), CD4⁺ (middle), and CD25⁺ (right) immune cell depleting antibodies ($n = 5-9$ mice per group). Statistical significance was determined using a log-rank test. (c) Tumour growth curves from mice treated as indicated. Tumour size (mm³) was measured over time from tumour inoculation and is shown here from the day of start of treatment until the first mouse of each group was euthanised. Statistical significance was determined using a mixed model ANOVA. Error bars represent the mean \pm SEM ($n = 5-9$ mice per group). (d) Representative immunofluorescence images of tumour tissue from a mouse treated with concomitant anti-VEGFR2 and anti-PD-L1 treatment (top) and a mouse treated with combo + CD4⁺ immune cell depletion (bottom), stained for CD31 (red) and DAPI (blue). 10x magnification. (e) heatmap of VECTASHIELD® analysis results expressed as the Fold change normalised to the concomitant treatment group. Statistical significance was determined by one-way ANOVA with Tukey's multiple comparisons test. * $p < 0.05$, ** $p < 0.01$, *** $p < 0.001$. Created with BioRender.com.

hand, CD4⁺ T cell depletion completely reversed the effect of combination treatment, with a statistically significant loss of tumor growth control ($p < 0.001$) (Figure 5c). Conversely, depletion of CD25⁺ Tregs significantly improved the therapeutic outcome compared to concomitant treatment with improved tumor growth control ($p = 0.023$) (Figure 5c). In addition, survival curves generally followed the same trend (aCD4 vs concomitant: $p = 0.0823$; aCD25 vs concomitant: $p = 0.0727$) (Figure 5b).

Based on literature,²⁷ we hypothesized that the attenuation of treatment efficacy in the absence of CD4⁺ T cells could be due to this cell population's apparent role in angiogenesis. As such, we performed additional immunofluorescent staining of the intratumoural blood vessels and observed a significant destabilization of the vasculature in the CD4⁺ depletion group (Figure 5d-e). In fact, compared to the non-depleted combination treatment group, CD4⁺ T cell depletion was associated with a significant reduction in CD31⁺ endothelial cells and a sparse vascular network with minimal branching and loop formation (Figure 5e). Interestingly, CD25 depletion also negatively impacted the intratumoural vasculature, albeit to a lesser extent (Figure 5e). These results highlight the critical role of CD4⁺ T cells in maintaining vascular stability and therapeutic efficacy, while Treg depletion suggests potential for improved treatment outcomes.

4. Discussion

The aggressive nature of PM is compounded by the associated complex tumor microenvironment, characterized by immune evasion and angiogenic processes. Understanding the interplay between immune checkpoints and angiogenesis is crucial for the development of more effective treatment options. In our study, we explored the effect of anti-VEGFR2 monoclonal antibody therapy, alone or in combination with anti-PD-L1 immune checkpoint blockade (ICB) in a syngeneic mouse model of mesothelioma, focusing on the association between tumor growth, immune cell infiltration, and vascular changes.

Consistent with several studies^{17,18,26,28} we found that high-dose (40 mg/kg) anti-VEGFR2 therapy significantly delayed tumor growth and improved survival in our mesothelioma model. These studies uniformly report that anti-VEGFR2 at this dose effectively inhibits tumor growth across different cancer types, including breast cancer,^{18,28} pancreatic neuroendocrine tumors,¹⁷ and hepatocellular carcinoma (HCC).²⁶ Notably, profound anti-tumor effects have also been observed with low-dose (10 mg/kg) anti-VEGFR2 when combined with anti-PD-1 ICB.²⁹ In fact, combining anti-angiogenic therapy with ICB agents like anti-PD-L1 or anti-PD-1 has been shown to further enhance tumor growth delay and improve survival in various murine models,^{17,18,26,30} aligning with our observations of better tumor control and survival with combination therapy. Additionally, we evaluated the effect of combining anti-VEGFR2 and anti-PD-L1 in a sequential manner. While we found that both induction and concomitant administrations of anti-VEGFR2 were superior to consolidation in PM, a study in Lewis lung carcinoma indicated that the induction setting resulted in reduced tumor volume compared to simultaneous

treatment.³¹ This confirms the importance of the order of compound administration in combination therapies.

Anti-VEGFR2 monotherapy led to a significant reduction in blood vessel length and a slight decrease in microvessel density (MVD), aligning with the anti-angiogenic effects observed in various tumor models.^{18,28,32} These studies consistently demonstrated that high-dose anti-VEGFR2 induces vascular regression and decreases vessel density across different cancer types. However, our combination treatment with high-dose anti-VEGFR2 and anti-PD-L1 produced different vascular effects. Notably, in our AE17 PM model this combination resulted in increased MVD, more branching points, longer vessel length, and more loops, indicating a shift toward vascular normalization rather than regression. This finding is consistent with reports by Sato et al.³¹ and Shigeta et al.,²⁶ where combined anti-angiogenic and immune checkpoint therapies promoted durable vascular formation and normalization in Lewis lung carcinoma and HCC, respectively. The increased vessel length and complexity observed in our study suggest that the combination treatment can enhance vascular maturation and remodeling, potentially improving therapeutic delivery and efficacy.

Pericyte coverage was notably enhanced when anti-VEGFR2 treatment was administered in the induction setting before anti-PD-L1. This sequential administration effect, enhancing vessel stability and normalization, aligns with findings from Winkler et al.³³ and Sato et al.,³¹ who reported increased pericyte coverage and structural vessel improvements following combined treatments in preclinical models of glioma and Lewis lung carcinoma, respectively.

Contrary to two studies that reported reduced hypoxia following vascular normalization,^{28,33} our study found no significant changes in hypoxia levels with either anti-VEGFR2 monotherapy or the combination treatment. This discrepancy might be due to the differences in experimental setup, such as tumor models and timing of hypoxia assessment. It is possible that hypoxia reduction might occur at earlier stages post-treatment, which we did not evaluate.

In summary, our combination treatment with high-dose anti-VEGFR2 and anti-PD-L1 resulted in increased MVD, more complex vascular structures, and improved pericyte coverage when administered sequentially, indicating significant vascular normalization. These effects contribute to the overall anti-tumor efficacy observed and highlight the intricate balance between anti-angiogenic and immune checkpoint therapies in modulating tumor vasculature.

Our finding that anti-VEGFR2 monotherapy increased Treg, CD4⁺ Th, and CD8⁺ T cell infiltration compares with the varied immune responses observed in studies on other tumor types. For example, Li et al.¹⁸ and Allen et al.¹⁷ reported increased CD8⁺ T cell infiltration in breast and pancreatic tumors, respectively, while Shigeta et al.²⁶ found a decrease in cytotoxic T lymphocytes (CTL) with high-dose anti-VEGFR2 treatment in HCC. It is worth noting, however, that infiltrating immune cell numbers in our experiments were low, and statistical significance reflected small absolute changes in cell numbers rather than a substantial biological effect. Interestingly, and in line with our observations, Tada et al.³⁰ also did not see an increase in infiltrating lymphocytes in

mouse mesothelioma tumors treated with anti-PD-1 and nintedanib. In addition, they observed a shift in the morphology of tumor-associated macrophages toward the more anti-tumor M1 phenotype, which would be an interesting venue to explore further.

We also identified a population of CD3⁺CD4⁺CD8[−] double-negative T (DNT) cells and a subset of CD4⁺CD25⁺FOXP3⁺ cells within tumors, neither of which significantly changed in response to treatment. DNT cells have been described as having both pro- and anti-tumor functions depending on the tumor context, and have been observed in several malignancies, including NSCLC, glioma, melanoma, and pancreatic cancer.^{34–38} Similarly, CD4⁺CD25⁺FOXP3⁺ cells have been suggested to represent a distinct subset of regulatory T cells with immunomodulatory functions.^{39,40} While their role in mesothelioma remains unclear, these immune subsets could play a role in shaping the TIME by influencing immune activation or suppression.

These variations suggest that the immune-modulatory effects of anti-VEGFR2 and ICB therapies are highly dependent on the tumor microenvironment and specific immune cell populations within different tumor types.

Depletion of CD4⁺ T cells, not CD8⁺ T cells, significantly reversed the therapeutic benefits of combined anti-VEGFR2 and anti-PD-L1 treatment in our mesothelioma model. This contrasts with findings showing that CD8⁺ T cell depletion abrogated the antitumoral effects of low-dose anti-VEGFR2 and anti-PD-1 in murine breast cancer,²⁹ highlighting the importance of CD4⁺ T cells in our model. Tian et al.²⁷ also emphasized the crucial role of CD4⁺ T cells, demonstrating that combined ICB targeting CTLA-4 and PD-1 in mouse mammary tumors still effectively delayed tumor growth even in the absence of CD8⁺ T cells.

While the predominance of CD4⁺ over CD8⁺ T cells in mediating therapeutic effects is uncommon in most murine tumor models, it may be partially explained by the antigen presentation characteristics of AE17 mesothelioma cells. Chang et al.⁴¹ assessed *in vitro* MHC expression in AE17 cells and found that while baseline expression of MHC I was very low (2.6%), it was substantially upregulated following IFN γ stimulation. In contrast, MHC II expression remained undetectable even after stimulation. These findings suggest that AE17 tumor cells are capable of presenting antigen to CD8⁺ T cells under inflammatory conditions, but may still be suboptimal targets compared to other models with high constitutive MHC I. This could contribute to the limited role of CD8⁺ T cells observed in our study. The absence of MHC II further supports the idea that CD4⁺ T cells likely act through indirect mechanisms, which may include the secretion of cytokines that shape the TME, modulation of other immune cells, or promotion of vascular normalization. While the Chang et al. study evaluated cultured AE17 cells and not *ex vivo* tumors, their findings offer a mechanistic rationale for the CD4-dominant response seen in our model.

CD4⁺ T cell depletion in our study led to reduced MVD and fewer vessel branching points, indicating a less mature and functional vascular architecture. This aligns with findings demonstrating that CD4⁺ T cells are essential for vascular remodeling and normal vessel formation in HCC models treated with combined anti-angiogenic and ICB therapy.²⁶

Similarly, CD4⁺ T cells have been found to play a critical role in supporting vascular normalization in breast tumor tissue,²⁷ further supporting our observations.

The depletion of Tregs in our study significantly improved survival and tumor growth control when combined with anti-PD-L1 and anti-VEGFR2, highlighting the immunosuppressive role of Tregs. This is consistent with studies showing that Treg depletion often results in a significant therapeutic benefit, particularly in combination with other immunomodulatory interventions such as ICB.^{42,43}

Regarding vasculature, Treg depletion in our study led to decreased MVD and fewer branching points, contributing to a less mature vasculature. This finding aligns with research demonstrating that Tregs can promote angiogenesis directly by upregulating VEGF-A levels^{44,45} and are required for lung angiogenesis.⁴⁶ Our results indicate that targeting Tregs can disrupt this process, underscoring the potential therapeutic benefit of Treg depletion to enhance the efficacy of anti-angiogenic and ICB therapies.

A key limitation of this study is the use of a subcutaneous tumor model rather than an orthotopic model of pleural mesothelioma. It is well established that tumor location can influence the TME and immune landscape, including immune cell infiltration, stromal interactions, and vascular dynamics.^{47,48} While our findings provide valuable insights into the immune and vascular effects of combined VEGFR2 and PD-L1 blockade, further studies in orthotopic models will be important to confirm the relevance of these mechanisms in the anatomical context of pleural mesothelioma.

Several ongoing clinical trials are exploring combinations of VEGFR2-targeting anti-angiogenic therapy and immune checkpoint inhibitors in non-small cell lung cancer (NSCLC). For instance, NCT03689855 is investigating atezolizumab (anti-PD-L1) combined with ramucirumab (anti-VEGFR2) in NSCLC patients who have progressed after prior ICB therapy, while NCT03527108 focuses on nivolumab (anti-PD-1) combined with ramucirumab in patients with recurrent, advanced metastatic NSCLC. Results from these trials are still pending but reflect a growing interest in dual targeting of angiogenesis and immune pathways. In mesothelioma, the phase 2 hCRN-LUN15-299 trial (NCT03502746) examined the combination of ramucirumab and nivolumab in patients with unresectable tumors after disease progression. Although this study did not meet its primary endpoint of a 40% objective response rate, the combination demonstrated favorable PFS and OS outcomes compared to single-agent nivolumab and was deemed safe with no increase in adverse effects relative to monotherapy.⁴⁹ Notably, this trial observed a better objective response rate in patients with non-epithelioid mesothelioma. Similarly, the BEAT-meso trial (NCT03762018) found that combined bevacizumab (anti-VEGF) + atezolizumab + chemotherapy significantly improved OS and PFS in the non-epithelioid but not the epithelioid subtype ($p = 0.0022$ and $p < 0.001$ versus $p = 0.97$ and $p = 0.060$, respectively; data presented at the ASCO Annual Meeting 2024). While this is in contrast with our findings in our murine

model of epithelioid mesothelioma, it is important to note that key differences in experimental setup such as therapeutic target (PD-1 versus PD-L1, VEGF versus VEGFR2) and administration route (systemic versus intraperitoneal), along with the inherent differences between human patients and murine models, could account for these discrepancies. As such, our study adds valuable insight into optimizing combination therapies for mesothelioma and underscores the importance of further preclinical research, particularly in the non-epithelioid histological subtype.

5. Conclusions

In conclusion, our study demonstrates that high-dose anti-VEGFR2, particularly in combination with anti-PD-L1, significantly enhances tumor growth control, survival, and vascular normalization in a mesothelioma mouse model. These findings underscore the critical role of the tumor microenvironment in shaping therapeutic responses and emphasize the potential of dual-targeting strategies to overcome the limitations of monotherapy. While our results align with prior research, they also reveal tumor-specific dynamics that could inform the design of more precise and effective treatments. This work paves the way for future investigations into dose optimization and combination regimens, with the goal of advancing therapeutic strategies for mesothelioma and improving clinical outcomes.

Acknowledgments

The authors wish to acknowledge Wesley Wilson and Caitlin Tilsed (NCARD, Perth, WA, Australia) for the development of and access to R scripts to perform mixed model ANOVA analyses. Conceptualisation, SR, JvM, EM and ES; formal analysis, SR, EM and SVL; funding acquisition, FL, JvM, EM and ES; investigation, SR, EM, SVL, MMR, LB, CH, HWL and CM; methodology, SR, EM, JVA, RV, PP, SVL and SF; project administration, SR, AW, EM and ES; resources, RV, SF, PP and SVL; supervision, JVA, FL, AW, JvM, EM and ES; validation, SR and EM; visualization, SR, EM, SVL and MMR; writing – original draft, SR; writing – review and editing, SR, JVA, RV, JDW, LB, CH, HWL, CM, MMR, PP, SVL, FL, AW, SF, JvM, EM and ES.

Author contributions

CRedit: **Sophie Rovers**: Conceptualization, Data curation, Formal analysis, Investigation, Methodology, Project administration, Validation, Visualization, Writing – original draft, Writing – review & editing; **Jonas Van Audenaerde**: Methodology, Supervision, Writing – review & editing; **Ruben Verloy**: Methodology, Resources, Writing – review & editing; **Jorrit De Waele**: Writing – review & editing; **Louize Brants**: Investigation, Writing – review & editing; **Christophe Hermans**: Investigation, Writing – review & editing; **Ho Wa Lau**: Investigation, Writing – review & editing; **Céline Merlin**: Investigation, Writing – review & editing; **Maria Möller Ribas**: Investigation, Visualization, Writing – review & editing; **Peter Ponsaerts**: Methodology, Resources, Writing – review & editing; **Steven Van Laere**: Formal analysis, Investigation, Methodology, Resources, Visualization, Writing – review & editing; **Filip Lardon**: Funding acquisition, Supervision, Writing – review & editing; **An Wouters**: Project administration, Supervision, Writing – review & editing; **Scott A. Fisher**: Methodology, Resources, Writing – review & editing; **Jan van Meerbeeck**: Conceptualization, Funding acquisition, Supervision, Writing – review & editing; **Elly Marcq**: Conceptualization, Formal analysis, Funding acquisition, Investigation, Methodology, Project administration, Supervision, Validation, Visualization, Writing – review & editing; **Evelien Smits**:

Conceptualization, Funding acquisition, Project administration, Supervision, Writing – review & editing.

Disclosure statement

No potential conflict of interest was reported by the author(s).

Funding

This research project has been funded by: Agentschap Innoveren en Ondernemen [OZ9869]; Fonds Wetenschappelijk Onderzoek [1SD6522N]; Kom op tegen Kanker [OZ8119]; Bijzonder Onderzoeksfonds UAntwerpen [FFB200053 and FFB210293]; We would like to thank several patrons, as part of the research and equipment was funded by donations from different donors, including Dedert Schilde vzw, Mr. Willy Floren and the Vereycken family.

ORCID

Sophie Rovers  <http://orcid.org/0000-0002-4936-859X>

Data availability statement

The datasets used and analyzed during the current study are available from the corresponding author on reasonable request.

Consent for publication

Not applicable.

Ethics approval and consent to participate

This study was conducted using publicly available data from The Cancer Genome Atlas (TCGA) database, which is fully anonymized and accessible to researchers in compliance with its data usage guidelines. As per the TCGA data access policy, no additional ethical approval or informed consent was required for this study. Detailed information about TCGA policies and guidelines can be found at <https://www.cancer.gov/ccg/research/genome-sequencing/tcga>. The authors hereby declare that in accordance with Belgian and European law, the use of anonymous data from a public database is not subjected to approval of an ethics committee.

Abbreviations

ANOVA	Analysis of variance
CTL	Cytotoxic T lymphocyte
DCs	Dendritic cells
DNT	Double-negative T cell
DFS	Disease-free survival
DSS	Disease-specific survival
FACS	Fluorescent activated cell sorting
FBS	Foetal bovine serum
HCC	Hepatocellular carcinoma
HR	Hazard ratio
i.p.	intraperitoneal
ICB	Immune checkpoint blockade
KDR	Kinase insert domain receptor
mAb	monoclonal antibody
mg	milligram
MHC	major histocompatibility complex
mm ³	cubic millimeter
MVD	microvessel density
NCARD	National Centre for Asbestos-Related Diseases
NK cell	Natural Killer cell
NSCLC	Non-small cell lung cancer

OS	Overall survival
PBS	Phosphate buffered saline
PD-1	Programmed cell death protein 1
PD-L1	Programmed death-ligand 1
PFS	Progression-free survival
PM	Pleural mesothelioma
Px	Pixel
s.c.	subcutaneous
SEM	Standard error of the mean
TCGA	The Cancer Genoma Atlas
Th cell	T helper cell
TIME	Tumour immune microenvironment
TIS	Tumour inflammation score
Treg	Regulatory T cell
VEGFA	Vascular endothelial growth factor A
VEGFR2	Vascular endothelial growth factor receptor 2
VST	Variance stabilizing transformation
αSMA	alpha-smooth muscle actin

References

- Scherpereel A, Astoul P, Baas P, Berghmans T, Clayson H, de Vuyst P, Dienemann H, Galateau-Salle F, Hennequin C, Hillerdal G, et al. Guidelines of the European respiratory society and the European society of thoracic surgeons for the management of malignant pleural mesothelioma. *Eur Respir J*. 2010;35(3):479–495. doi: [10.1183/09031936.00063109](https://doi.org/10.1183/09031936.00063109).
- Bonelli MA, Fumarola C, La Monica S, Alfieri R. New therapeutic strategies for malignant pleural mesothelioma. *Biochemical Pharmacol*. 2017;123:8–18. doi: [10.1016/j.bcp.2016.07.012](https://doi.org/10.1016/j.bcp.2016.07.012).
- Lococo F. Malignant pleural mesothelioma: time is running out. *J Clin Med*. 2021;10(4): 648. doi: [10.3390/jcm10040648](https://doi.org/10.3390/jcm10040648).
- Chimed-Ochir O, Rath E-M, Kubo T, Yumiya Y, Lin R-T, Furuya S, Brislane K, Klebe S, Nowak AK, Kang SK, Takahashi K. Must countries shoulder the burden of mesothelioma to ban asbestos? A global assessment. *BMJ Glob Health*. 2022;7(12): e010553. doi: [10.1136/bmjgh-2022-010553](https://doi.org/10.1136/bmjgh-2022-010553).
- Opitz I, Bille A, Dafni U, Nackaerts K, Ampollini L, de Perrot M, Bric L, Nadal E, Syrigos K, Gray SG, et al. European epidemiology of pleural mesothelioma—real-Life data from a joint analysis of the mesoscape database of the European thoracic oncology platform and the European society of thoracic surgery mesothelioma database. *J Thorac Oncol*. 2023;18(9):1233–1247. doi: [10.1016/j.jtho.2023.06.011](https://doi.org/10.1016/j.jtho.2023.06.011).
- European Commission, Directorate-General for Employment, Social Affairs, and Inclusion, Lassen C, Christens F, Vencovska, J. Study on collecting information on substances with the view to analyse health, socio-economic and environmental impacts in connection with possible amendments of directive 98/24/EC (chemical agents) and directive 2009/148/EC (asbestos) – final report for asbestos. Publications Office; 2021.
- van Meerbeeck JP, Scherpereel A, Surmont VF, Baas P. Malignant pleural mesothelioma: the standard of care and challenges for future management. *Crit Rev In Oncol/Hematol*. 2011;78(2):92–111. doi: [10.1016/j.critrevonc.2010.04.004](https://doi.org/10.1016/j.critrevonc.2010.04.004).
- Vogelzang NJ, Rusthoven JJ, Symanowski J, Denham C, Kaukel E, Ruffie P, Gatzemeier U, Boyer M, Emri S, Manegold C, et al. Phase III study of pemetrexed in combination with cisplatin versus cisplatin alone in patients with malignant pleural mesothelioma. *J Clin Oncol*. 2003;21(14):2636–2644. doi: [10.1200/JCO.2003.11.136](https://doi.org/10.1200/JCO.2003.11.136).
- Baas P, Scherpereel A, Nowak AK, Fujimoto N, Peters S, Tsao AS, Mansfield AS, Popat S, Jahan T, Antonia S, et al. First-line nivolumab plus ipilimumab in unresectable malignant pleural mesothelioma (CheckMate 743): a multicentre, randomised, open-label, phase 3 trial. *Lancet*. 2021;397(10272):375–386. doi: [10.1016/S0140-6736\(20\)32714-8](https://doi.org/10.1016/S0140-6736(20)32714-8).
- Sharma P, Allison JP. The future of immune checkpoint therapy. *Science*. 2015;348(6230):56–61. doi: [10.1126/science.aaa8172](https://doi.org/10.1126/science.aaa8172).
- Rovers S, Janssens A, Raskin J, Pauwels P, van Meerbeeck JP, Smits E, Marcq E. Recent advances of immune checkpoint inhibition and potential for (combined) TIGIT blockade as a new strategy for malignant pleural mesothelioma. *Biomedicines*. 2022;10(3):673. doi: [10.3390/biomedicines10030673](https://doi.org/10.3390/biomedicines10030673).
- Zalcman G, Mazieres J, Margery J, Greillier L, Audigier-Valette C, Moro-Sibilot D, Molinier O, Corre R, Monnet I, Gounant V, et al. Bevacizumab for newly diagnosed pleural mesothelioma in the mesothelioma avastin cisplatin pemetrexed study (MAPS): a randomised, controlled, open-label, phase 3 trial. *Lancet*. 2016;387(10026):1405–1414. doi: [10.1016/S0140-6736\(15\)01238-6](https://doi.org/10.1016/S0140-6736(15)01238-6).
- Scagliotti GV, Gaafar R, Nowak AK, Nakano T, van Meerbeeck J, Popat S, Vogelzang NJ, Grosso F, Aboelhasan R, Jakopovic M, et al. Nintedanib in combination with pemetrexed and cisplatin for chemotherapy-naïve patients with advanced malignant pleural mesothelioma (LUME-Meso): a double-blind, randomised, placebo-controlled phase 3 trial. *Lancet Respir Med*. 2019;7(7):569–580. doi: [10.1016/S2213-2600\(19\)30139-0](https://doi.org/10.1016/S2213-2600(19)30139-0).
- Pinto C, Zucali PA, Pagano M, Grosso F, Pasello G, Garassino MC, Tiseo M, Soto Parra H, Grossi F, Cappuzzo F, et al. Gemcitabine with or without ramucirumab as second-line treatment for malignant pleural mesothelioma (RAMES): a randomised, double-blind, placebo-controlled, phase 2 trial. *Lancet Oncol*. 2021;22(10):1438–1447. doi: [10.1016/S1470-2045\(21\)00404-6](https://doi.org/10.1016/S1470-2045(21)00404-6).
- Miettinen M, Rikala M-S, Rys J, Lasota J, Wang Z-F. Vascular endothelial growth factor receptor 2 as a marker for malignant vascular tumors and mesothelioma: an immunohistochemical study of 262 vascular endothelial and 1640 nonvascular tumors. *Am J Surg Pathol*. 2012;36(4):629–639. doi: [10.1097/PAS.0b013e318243555b](https://doi.org/10.1097/PAS.0b013e318243555b).
- Laszlo V, Valko Z, Kovacs I, Ozsvar J, Hoda MA, Klikovits T, Lakatos D, Czirik A, Garay T, Stiglbauer A, et al. Nintedanib is active in malignant pleural mesothelioma cell models and inhibits angiogenesis and tumor growth in vivo. *Clin Cancer Res*. 2018;24(15):3729–3740. doi: [10.1158/1078-0432.CCR-17-1507](https://doi.org/10.1158/1078-0432.CCR-17-1507).
- Allen E, Jabouille A, Rivera LB, Lodewijckx I, Missiaen R, Steri V, Feyen K, Tawney J, Hanahan D, Michael IP, et al. Combined antiangiogenic and anti-PD-L1 therapy stimulates tumor immunity through HEV formation. *Sci Transl Med*. 2017;9(385). doi: [10.1126/scitranslmed.aak9679](https://doi.org/10.1126/scitranslmed.aak9679).
- Li Y, Amaladas N, O'Mahony M, Manro JR, Inigo I, Li Q, Rasmussen ER, Brahmachary M, Doman TN, Hall G, et al. Treatment with a VEGFR-2 antibody results in intra-tumor immune modulation and enhances anti-tumor efficacy of PD-L1 blockade in syngeneic murine tumor models. *PLOS ONE*. 2022;17(7):e0268244. doi: [10.1371/journal.pone.0268244](https://doi.org/10.1371/journal.pone.0268244).
- Marcq E, Van Audenaerde JRM, De Waele J, Merlin C, Pauwels P, van Meerbeeck JP, Fisher SA, Smits ELJ. The search for an interesting partner to combine with PD-L1 blockade in mesothelioma: focus on TIM-3 and LAG-3. *Cancers*. 2021;13(2):282. doi: [10.3390/cancers13020282](https://doi.org/10.3390/cancers13020282).
- Fear VS, Tilsed C, Chee J, Forbes CA, Casey T, Solin JN, Lansley SM, Lesterhuis WJ, Dick IM, Nowak AK, et al. Combination immune checkpoint blockade as an effective therapy for mesothelioma. *Oncoimmunology*. 2018;7(10):e1494111. doi: [10.1080/2162402X.2018.1494111](https://doi.org/10.1080/2162402X.2018.1494111).
- Shaheen RM, Ahmad SA, Liu W, Reinmuth N, Jung YD, Tseng WW, Drazan KE, Bucana CD, Hicklin DJ, Ellis LM, et al. Inhibited growth of colon cancer carcinomas by antibodies to vascular endothelial and epidermal growth factor receptors. *Br J Cancer*. 2001;85(4):584–589. doi: [10.1054/bjoc.2001.1936](https://doi.org/10.1054/bjoc.2001.1936).
- He B, Johansson-Percival A, Backhouse J, Li J, Lee GYF, Hamzah J, Ganss R. Remodeling of metastatic vasculature reduces lung colonization and sensitizes overt metastases to immunotherapy. *Cell Rep*. 2020;30(3):714–24.e5. doi: [10.1016/j.celrep.2019.12.013](https://doi.org/10.1016/j.celrep.2019.12.013).
- Ayers M, Lunceford J, Nebozhyn M, Murphy E, Loboda A, Kaufman DR, Albright A, Cheng JD, Kang SP, Shankaran V, et al. IFN-γ-related mRNA profile predicts clinical response to PD-1 blockade. *J Clin Invest*. 2017;127(8):2930–2940. doi: [10.1172/JCI91190](https://doi.org/10.1172/JCI91190).

24. Fisher SA, Peddle-McIntyre CJ, Burton K, Newton RU, Marcq E, Lake RA, Nowak AK. Voluntary exercise in mesothelioma: effects on tumour growth and treatment response in a murine model. *BMC Res Notes*. 2020;13(1):435. doi: [10.1186/s13104-020-05284-y](https://doi.org/10.1186/s13104-020-05284-y).
25. Danaher P, Warren S-O, Lu R, Samayoa J, Sullivan A, Pekker I, Wallden B, Marincola FM, Cesano A. Pan-cancer adaptive immune resistance as defined by the tumor inflammation signature (TIS): results from the cancer genome atlas (TCGA). *J For Immunother Cancer*. 2018;6(1). doi: [10.1186/s40425-018-0367-1](https://doi.org/10.1186/s40425-018-0367-1).
26. Shigeta K, Datta M, Hato T, Kitahara S, Chen IX, Matsui A, Kikuchi H, Mamessier E, Aoki S, Ramjiawan RR, et al. Dual programmed death receptor-1 and vascular endothelial growth factor receptor-2 blockade promotes vascular normalization and enhances antitumor immune responses in hepatocellular carcinoma. *Hepatology*. 2020;71(4):1247–1261. doi: [10.1002/hep.30889](https://doi.org/10.1002/hep.30889).
27. Tian L, Goldstein A, Wang H, Ching Lo H, Sun Kim I, Welte T, Sheng K, Dobrolecki LE, Zhang X, Putluri N, Phung TL, Mani SA, Stossi F, Sreekumar A, Mancini MA, Decker WK, Zong C, Lewis MT, Zhang XH. Mutual regulation of tumour vessel normalization and immunostimulatory reprogramming. *Nature*. 2017;544(7649):250–254. doi: [10.1038/nature21724](https://doi.org/10.1038/nature21724).
28. Huang Y, Yuan J, Righi E, Kamoun WS, Ancukiewicz M, Nezivar J, Santosuosso M, Martin J.D., Martin M.R., Vianello F, Leblanc P, Munn LL, Huang P, Duda DG, Fukumura D, Jain RK, Poznansky MC. Vascular normalizing doses of antiangiogenic treatment reprogram the immunosuppressive tumor microenvironment and enhance immunotherapy. *Proceedings of the National Academy of Sciences of the United States of America*; Vol. 109(43):2012. p. 17561–17566. doi: [10.1073/pnas.1215397109](https://doi.org/10.1073/pnas.1215397109).
29. Li Q, Wang Y, Jia W, Deng H, Li G, Deng W, Chen J, Kim BYS, Jiang W, Liu Q, et al. Low-dose anti-angiogenic therapy sensitizes breast cancer to PD-1 blockade. *Clin Cancer Res*. 2020;26(7):1712–1724. doi: [10.1158/1078-0432.CCR-19-2179](https://doi.org/10.1158/1078-0432.CCR-19-2179).
30. Tada A, Minami T, Kitai H, Higashiguchi Y, Tokuda M, Higashiyama T, Negi Y, Horio D, Nakajima Y, Otsuki T, et al. Combination therapy with anti-programmed cell death 1 antibody plus angiokinase inhibitor exerts synergistic antitumor effect against malignant mesothelioma via tumor microenvironment modulation. *Lung Cancer*. 2023;180:107219. doi: [10.1016/j.lungcan.2023.107219](https://doi.org/10.1016/j.lungcan.2023.107219).
31. Sato M, Maishi N, Hida Y, Yanagawa-Matsuda A, Alam MT, Sakakibara-Konishi J, Nam J-M, Onodera Y, Konno S, Hida K, et al. Angiogenic inhibitor pre-administration improves the therapeutic effects of immunotherapy. *Cancer Med*. 2023;12(8):9760–9773. doi: [10.1002/cam4.5696](https://doi.org/10.1002/cam4.5696).
32. Tong RT, Boucher Y, Kozin SV, Winkler F, Hicklin DJ, Jain RK. Vascular normalization by vascular endothelial growth factor receptor 2 blockade induces a pressure gradient across the vasculature and improves drug penetration in tumors. *Cancer Res*. 2004;64(11):3731–3736. doi: [10.1158/0008-5472.CAN-04-0074](https://doi.org/10.1158/0008-5472.CAN-04-0074).
33. Winkler F, Kozin SV, Tong RT, Chae S-S, Booth MF, Garkavtsev I, Xu L, Hicklin D, Fukumura D, Ditomaso E, et al. Kinetics of vascular normalization by VEGFR2 blockade governs brain tumor response to radiation: Role of oxygenation, angiopoietin-1, and matrix metalloproteinases. *Cancer Cell*. 2004;6(6):553–563. doi: [10.1016/S1535-6108\(04\)00305-8](https://doi.org/10.1016/S1535-6108(04)00305-8).
34. Wu Z, Zheng Y, Sheng J, Han Y, Yang Y, Pan H, Yao J. CD3+CD4-CD8- (double-negative) T cells in inflammation, immune disorders and cancer. *Front Immunol*. 2022;13:816005. doi: [10.3389/fimmu.2022.816005](https://doi.org/10.3389/fimmu.2022.816005).
35. Fang L, Ly D, Wang SS, Lee JB, Kang H, Xu H, Yao J, Tsao M-S, Liu W, Zhang L. Targeting late-stage non-small cell lung cancer with a combination of DNT cellular therapy and PD-1 checkpoint blockade. *J Exp Clin Cancer Res*. 2019;38(1):123. doi: [10.1186/s13046-019-1126-y](https://doi.org/10.1186/s13046-019-1126-y).
36. Prins RM, Incardona F, Lau R, Lee P, Claus S, Zhang W, Black KL, Wheeler CJ. Characterization of defective CD4–CD8– T cells in murine tumors generated Independent of antigen specificity. *J Immunol*. 2004;172(3):1602–1611. doi: [10.4049/jimmunol.172.3.1602](https://doi.org/10.4049/jimmunol.172.3.1602).
37. Mondragón L, Kroemer G, Galluzzi L. Immunosuppressive γδ T cells foster pancreatic carcinogenesis. *Oncoimmunology*. 2016;5(11):e1237328. doi: [10.1080/2162402X.2016.1237328](https://doi.org/10.1080/2162402X.2016.1237328).
38. Daley D, Zambirinis CP, Seifert L, Akkad N, Mohan N, Werba G, Barilla R, Torres-Hernandez A, Hundeyin M, Mani VRK, et al. γδ T cells support pancreatic oncogenesis by restraining αβ T cell activation. *Cell*. 2016;166(6):1485–99.e15. doi: [10.1016/j.cell.2016.07.046](https://doi.org/10.1016/j.cell.2016.07.046).
39. Hu X, Gu Y, Zhao S, Hua S, Jiang Y. Elevated circulating CD4+CD25–Foxp3+ regulatory T cells in patients with nonsmall cell lung cancer. *Cancer Biother Radiopharm*. 2019;34(5):325–333. doi: [10.1089/cbr.2018.2672](https://doi.org/10.1089/cbr.2018.2672).
40. Zelenay S, Lopes-Carvalho T, Caramalho I, Moraes-Fontes MF, Rebelo M, Demengeot J. Foxp3 + CD25 – CD4 T cells constitute a reservoir of committed regulatory cells that regain CD25 expression upon homeostatic expansion. *Proc Natl Acad Sci USA*. 2005;102(11):4091–4096. doi: [10.1073/pnas.0408679102](https://doi.org/10.1073/pnas.0408679102).
41. Chang F, Keam S, Hoang TS, Creaney J, Gill S, Nowak AK, Ebert M, Cook AM. Immune marker expression of irradiated mesothelioma cell lines. *Front Oncol*. 2022;12:1020493. doi: [10.3389/fonc.2022.1020493](https://doi.org/10.3389/fonc.2022.1020493).
42. Suttmüller RP, van Duivenvoorde LM, van Elsas A, Schumacher TN, Wildenberg ME, Allison JP, Toes REM, Offringa R, Melief CJM. Synergism of cytotoxic T lymphocyte-associated antigen 4 blockade and depletion of CD25+ regulatory T cells in antitumor therapy reveals alternative pathways for suppression of autoreactive cytotoxic T lymphocyte responses. *J Exp Med*. 2001;194(6):823–832. doi: [10.1084/jem.194.6.823](https://doi.org/10.1084/jem.194.6.823).
43. Bos PD, Plitas G, Rudra D, Lee SY, Rudensky AY. Transient regulatory T cell ablation deters oncogene-driven breast cancer and enhances radiotherapy. *J Exp Med*. 2013;210(11):2435–2466. doi: [10.1084/jem.20130762](https://doi.org/10.1084/jem.20130762).
44. Facciabene A, Motz GT, Coukos G. T-regulatory cells: key players in tumor immune escape and angiogenesis. *Cancer Res*. 2012;72(9):2162–2171. doi: [10.1158/0008-5472.CAN-11-3687](https://doi.org/10.1158/0008-5472.CAN-11-3687).
45. Facciabene A, Peng X, Hagemann I, Balint K, Wang L, Gimmoty P, Gilks CB, Lal P, Zhang L, Coukos G. Tumour hypoxia promotes tolerance and angiogenesis via CCL28 and T(reg) cells. *Nature*. 2012;475(7355):226–30. doi: [10.1038/nature10169](https://doi.org/10.1038/nature10169).
46. D'Alessio FR, Zhong Q, Jenkins J, Moldobaeva A, Wagner EM. Lung angiogenesis requires CD4+ forkhead homeobox protein-3+ regulatory T cells. *Am J Respir Cell Mol Biol*. 2015;52(5):603–610. doi: [10.1165/rcmb.2014-0278OC](https://doi.org/10.1165/rcmb.2014-0278OC).
47. Stribbling SM, Beach C, Ryan AJ. Orthotopic and metastatic tumour models in preclinical cancer research. *Pharmacology & Therapeutics*. 2024;257:108631. doi: [10.1016/j.pharmthera.2024.108631](https://doi.org/10.1016/j.pharmthera.2024.108631).
48. Gengenbacher N, Singhal M, Augustin HG. Preclinical mouse solid tumour models: status quo, challenges and perspectives. *Nat Rev Cancer*. 2017;17(12):751–765. doi: [10.1038/nrc.2017.92](https://doi.org/10.1038/nrc.2017.92).
49. Dudek AZ, Xi MX, Scilla KA, Mamdani H, Creelan BC, Saltos A, Tanvetyanon T, Chiappori A. Phase 2 trial of Nivolumab and ramucirumab for relapsed mesothelioma: HCRN-LUN15-299. *JTO Clin & Res Rep*. 2023;4(12):100584. doi: [10.1016/j.jtocrr.2023.100584](https://doi.org/10.1016/j.jtocrr.2023.100584).